Photoacoustic characterization of semiconductors: Transport properties and thermal diffusivity in GaAs and Si

A. Pinto Neto and H. Vargas
Instituto de Física, Universidade Estadual de Campinas, Caixa Postal 1170, 13 100 Campinas, São Paulo, Brazil

N. F. Leite and L. C. M. Miranda
Laboratório Associado de Sensores e Materiais (LAS), Instituto de Pesquisas Espaciais (INPE), Caixa Postal 515, 12 201 São José dos Campos, São Paulo, Brazil

(Received 20 November 1989)

The photoacoustic signal of two semiconductor samples is investigated as a function of the modulation frequency in a heat-transmission configuration. It is shown that, in the frequency range where the sample is thermally thick, the signal amplitude and phase can single out the different fast and slow nonradiative recombination heat sources responsible for the photoacoustic signal. The characterization of the thermal and the carrier transport properties is discussed and some practical procedures for this purpose are also outlined.

INTRODUCTION

Thermal-wave physics is becoming a valuable tool in the study of material parameters as well as in the semiconductor industry for characterizing processes in the manufacturing of electronic devices.[1-3] These waves are created whenever there is a periodic heat generation in a medium. The most common mechanism for producing thermal waves is the absorption of an intensity modulated light beam by a sample. Of the several mechanisms[3] available for detecting these waves, the gas-microphone photoacoustic (PA) detection is the most widely used so far. In this case a sample is placed in a small, air-tight cell, at a given distance from a transparent window through which a light beam is incident upon the sample. As a result of the light-into-heat conversion, the sample is heated by the absorption of the modulated light beam. The heat flow from the sample to the surrounding air causes the pressure in the air chamber to fluctuate, which is sensed by a microphone mounted in one of the lateral cell walls.

Being a photothermal technique, the detected signal is strongly dependent upon the interplay of the sample optical-absorption coefficient for the incident radiation, the light-into-heat conversion efficiency, as well as how the heat diffuses through the sample. The dependence of the PA signal on the absorption coefficient allows us to perform spectroscopic studies, whereas the fact that the signal is proportional to the light-into-heat conversion efficiency means that it is complementary to other photoinduced energy-conversion processes. This means that the PA detection can be used for obtaining information concerning the nonthermal deexcitation processes. Finally, the fact that the PA signal depends on how the heat diffuses through the sample allows us to perform both thermal characterization of the sample (i.e., measurements of its thermal properties, such as thermal diffusivity and thermal conductivity), and thermal imaging. In the case of semiconductors, the PA signal provides us with additional information regarding the carrier-transport properties, a fact which has been recognized since the earlier PA studies in semiconductors.[4-9] Qualitatively, this may be understood as follows. The absorption of radiation with photon energy $h\nu$ greater than the band-gap energy E_g creates an excess carrier distribution in the sample with an energy $h\nu - E_g$ above the conduction band. In a time scale of a few picoseconds these photoinjected carriers give off this excess energy to the lattice by relaxing to the bottom of the conduction band via the electron-phonon collisions within the conduction band. At this point the excess carriers diffuse through the sample and reestablish equilibrium by disposing of the energy E_g in excess to the lattice by recombining with the holes in the valence band.

In this paper we investigate the carrier transport properties (or carrier diffusion coefficient, surface recombination velocity, and bulk recombination time) as well as the thermal diffusivity of two semiconductors (GaAs and Si) and of a silicon solar cell using the recently proposed open-photoacoustic-cell (OPC) detection technique.[10,11]

EXPERIMENT

The OPC experimental apparatus is schematically shown in Fig. 1(a). The mechanically modulated light beam from a 250-W tungsten filament lamp is focused onto the sample. The white light is filtered for wavelengths greater than 800 nm using a heat filter so that the light absorption may be assumed to take place at the front surface of the samples. The samples are mounted directly onto the front sound inlet of an electret microphone. The sound inlet is a circular hole of 3 mm diameter, and the front microphone air chamber adjacent to the metallized face of the diaphragm is a cylinder of 7 mm diameter and roughly 1 mm long. Except for sample 1 below, all the measurements were carried out with

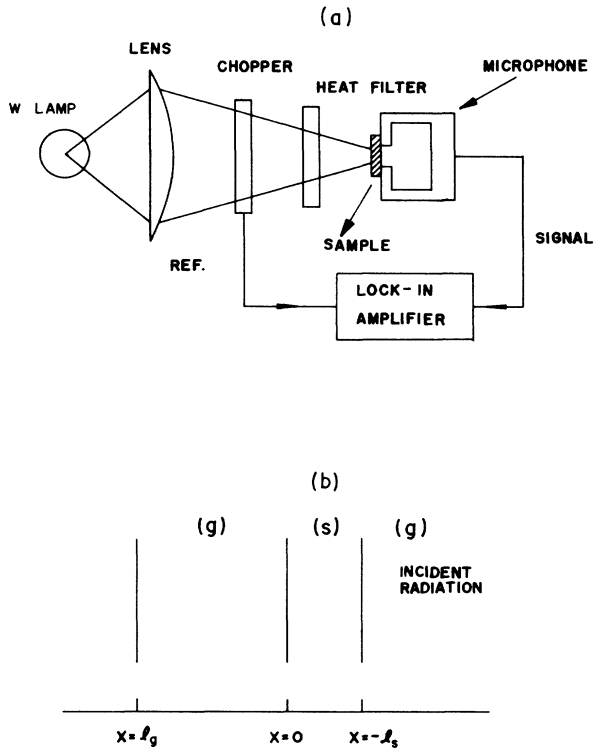

FIG. 1. (a) Experimental arrangement use in the OPC measurements, and (b) PA cell geometry for the heat transmission configuration.

heat-filtered white-light illumination. In the case of sample 1 we have used a 180-mW Ar^+-ion laser as the heating beam.

The samples used were two n-type GaAs ($N_d \simeq 5\times10^{17}$ cm^{-3}) sample, two 5×5 mm^2 Si solar cells, and a p-type Si ($N_a \simeq 1.5\times10^{14}$ cm^{-3}). To investigate the influence of the surface recombination velocity on the PA signal, the sample surface had different finishings. For the n-type GaAs sample we had two different surface finishings. For one sample ($N_d \simeq 5\times10^{17}$ cm^{-3}), sample 1, both surfaces were previously roughened by polishing them with 9-μm mesh Al_2O_3 abrasive powder. This was follow by the deposition of a 1000-Å-thick Au film on the back surface facing the OPC chamber. The sample was then annealed at 700 °C for 30 s. In this way a fast surface recombination velocity at the back surface was assured. For the other n-type GaAs sample, $N_d \simeq 10^{18}$ cm^{-3}, the surface finishings were obtained by mechanical polishing. One finish, henceforth called polished surface (PS), was a mirrorlike finish obtained by a sequence of mechanical polishing using Al_2O_3 powder of different meshes (9, 5, and 2 μm) followed by polishing in a flannel embedded in iodine methanol solution surface. The roughened-surface (RS) finish was obtained using the 9-μm mesh Al_2O_3 polishing; the surface finishing for the p-type Si sample was produced by mechanical polishing as described above. To investigate the bulk and surface nonradiative processes in Si solar cell, we have used cells with different back-surface characteristics, namely, one with a back-surface field (BSF) and the other one with no BSF. The 5×5 mm^2 solar cells were manufactured from p-type substrate (B-doped, $p \simeq 10$ Ω cm) with p-type implanted junction (junction depth of roughly 0.2 to 0.3 μm). The front surface had a TiO_2 antireflecting coating with minimum reflectance at 550 nm. The front electrode was made of Tl ($\simeq 0.1$ μm)-Pd($\simeq 1$ μm)-Ag($\simeq 4$ μm) alloy whereas the back electrode consisted of Ti-Au alloy. The back-surface field was produced by B implantation. In Table I we summarize the physical parameters and surface state of the GaAs and Si samples used in this work. For samples 2–6 we shall denote their surface states by the corresponding notation for the front (heating) and rear surfaces. For example, sample 2 is a RS-RS GaAS sample, whereas sample 5 is a PS-RS Si sample.

In Fig. 2 we show the OPC signal amplitude for sample 1 as a function of the modulation frequency. We note that in the frequency range of our experiment, using the literature value[12] of the thermal diffusivity of GaAS (i.e., $\alpha=0.44$ cm^2/s), sample 1 is thermally thick; i.e., its thermal diffusion length $(\alpha/\pi f)^{1/2}$, where f is the modulation frequency, is much smaller than its thickness l. The solid lines in this figure represent the best fit to the data by a power law, i.e., signal $\sim f^{-\nu}$. This fitting procedure led to the conclusion that between 350 and 550 Hz, the OPC signal of sample 1 behaves as $f^{-1.5}$, whereas between 650 and 800 Hz it follows a $f^{-1.0}$ power law. In Figs. 3–5 we show the dependence of the OPC signal amplitude as a function of the modulation frequency for samples 2–4, respectively. In Fig. 3, the signal scales as $f^{-1.7}$ between 350 and 800 Hz, and as $f^{-1.1}$ between 900 and 1500 Hz. The same type of behavior is also exhibited by the PS-RS CaAS in Fig. 4 where the signal varies as $f^{-1.6}$ between 350 and 1150 Hz and as $f^{-1.2}$ between 1200 and 1500 Hz. However, for the PS-PS

TABLE I. Thickness, resistivity, and surface state of the front (heating) and rear surfaces of the GaAs and Si samples used in this work.

	Sample	Thickness (μm)	Doping concentration (cm^{-3})	Front surface	Rear surface
n-type GaAs	1	583	5.2×10^{17}	Roughened	Annealed Au film
n-type GaAs	2	420	$\sim10^{18}$	Roughened	Roughened
n-type GaAs	3	358	$\sim10^{18}$	Polished	Roughened
n-type GaAs	4	200	$\sim10^{18}$	Polished	Polished
p-type Si	5	388	1.5×10^{14}	Polished	Roughened
p-type Si	6	386	1.5×10^{14}	Roughened	Roughened

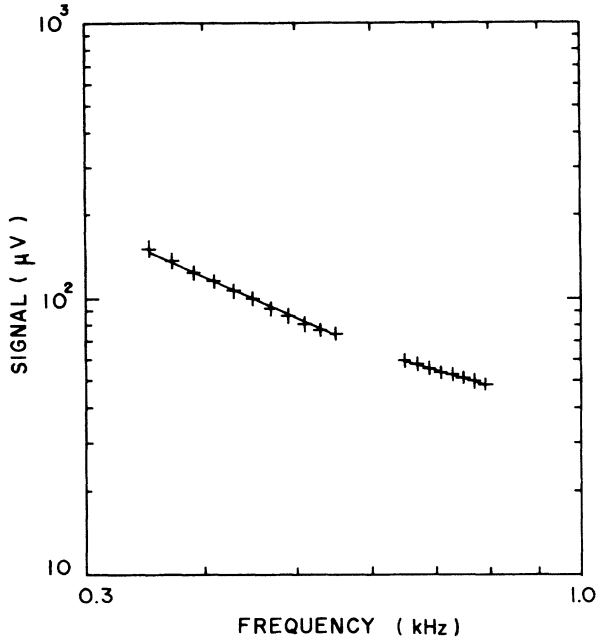

FIG. 2. OPC signal amplitude for sample 1 as a function of the modulation frequency.

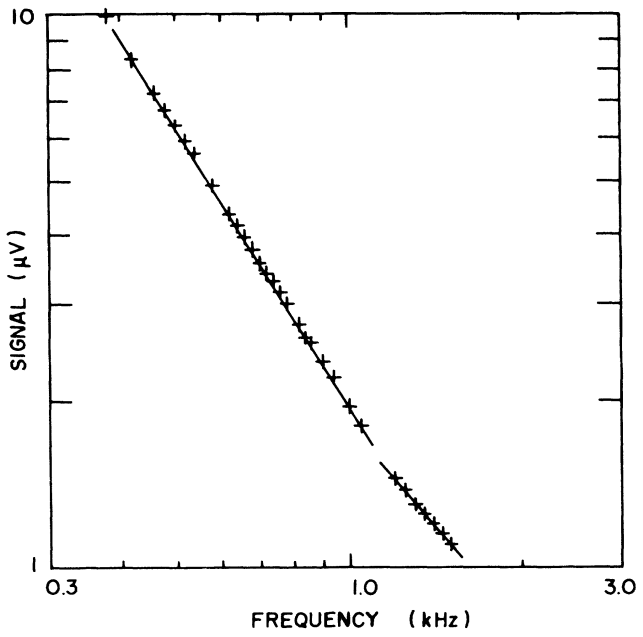

FIG. 4. OPC signal amplitude for sample 3 as a function of the modulation frequency.

GaAs sample shown in Fig. 5, the OPC signal exhibited an $f^{-1.44}$ dependence in the entire frequency range (580–1900 Hz) of our measurements. The first conclusion we can draw from the results shown in Figs. 2–4 is that whenever the rear surface has a fast carrier recombination velocity, as implied by the roughened-surface state, the OPC signal changes from an $f^{-1.5}$ to an $f^{-1.0}$ power law as one increases the modulation frequency. However, when the rear surface is a polished surface, which entails a slow carrier recombination velocity, the OPC signal amplitude tends to exhibit the $f^{-1.5}$ frequency dependence. Furthermore, the change from the $f^{-1.5}$ to the $f^{-1.0}$ frequency dependence of the OPC signal amplitude is also accompanied by a minimum in the OPC signal phase centered roughly at the modulation frequency where the signal amplitude changes from $f^{1.5}$ to the $f^{-1.0}$ dependence. In Figs. 6 and 7 we show the OPC signal phase of samples 1 and 2, respectively, as a function of the modulation frequency. We note from these figures that in the frequency range where the signal am-

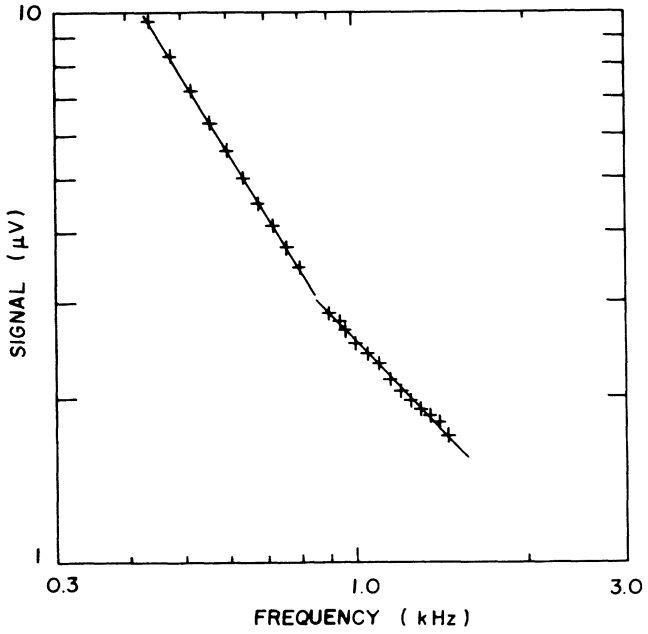

FIG. 3. OPC signal amplitude for sample 2 as a function of the modulation frequency.

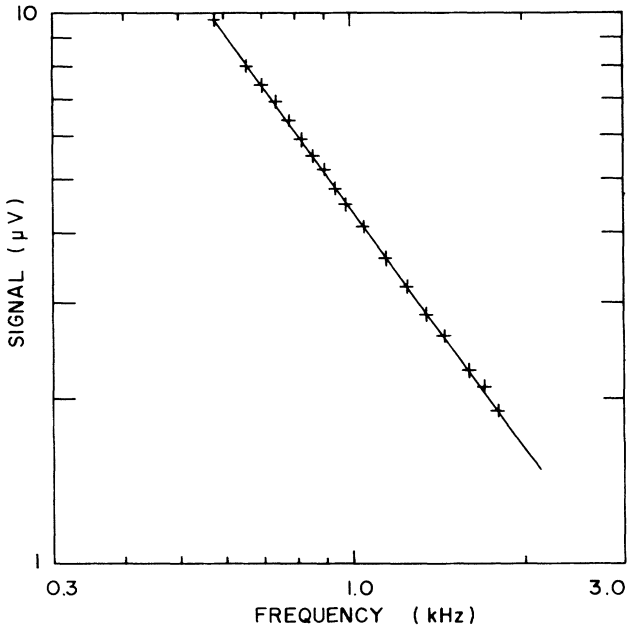

FIG. 5. OPC signal amplitude for sample 4 as a function of the modulation frequency.

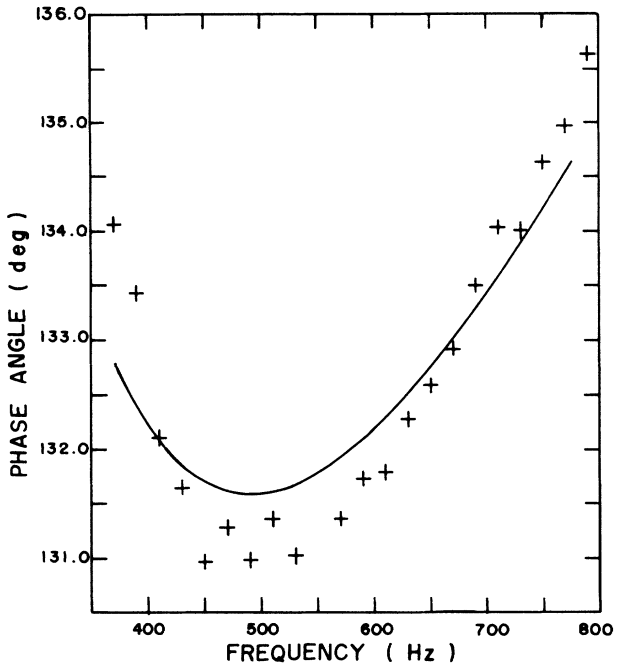

FIG. 6. OPC phase angle for sample 1 vs the modulation frequency. The solid line represents the data fitting to Eq. (11) of the text.

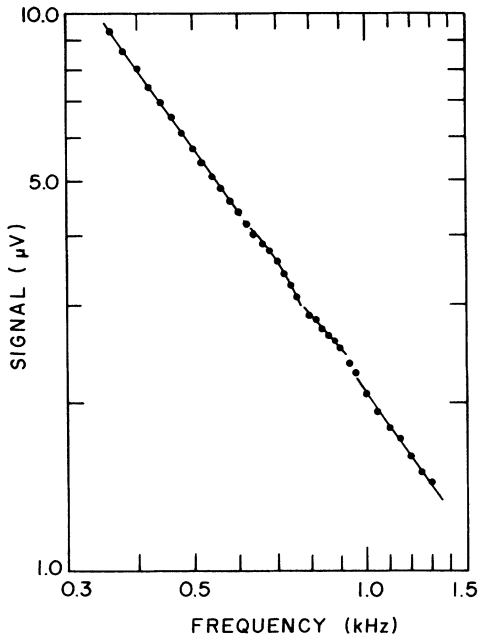

FIG. 8. OPC signal amplitude for the solar cell without BSF as a function of the modulation frequency.

plitude follows the $f^{-1.5}$ frequency dependence, the signal phase is a decreasing function of the modulation frequency, whereas when the signal amplitude behaves as $f^{-1.0}$, the phase angle increases with the modulation frequency. In contrast, when the rear surface is polished, such that the signal amplitude is always following the $f^{-1.5}$ power law, the phase angle is a monotonically decreasing function of the modulation frequency.

The results of the modulation frequency dependence for the solar cells are plotted in Figs. 8 and 9, for 240-μm-thick Si solar cell without BSF and the 235-μm-thick Si solar cell with BSF, respectively. Figure 8 shows that, for the solar cell without BSF, OPC signal amplitude exhibits four distinct modulation frequency dependences,

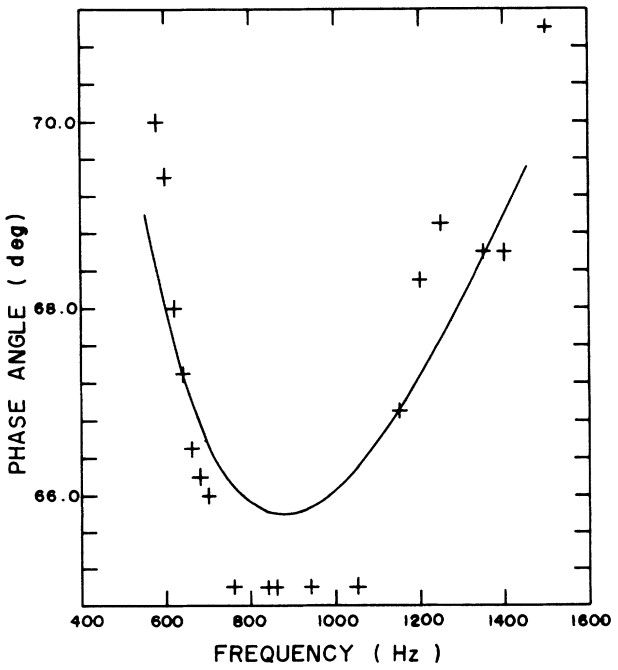

FIG. 7. OPC phase angle for sample 2 vs the modulation frequency. The solid line represents the data fitting to Eq. (11) of the text.

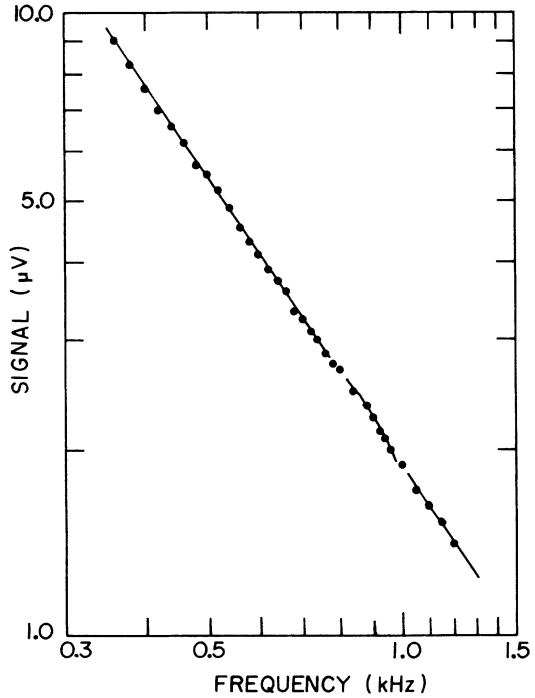

FIG. 9. OPC signal amplitude for the solar cell with BSF as a function of the modulation frequency.

namely, an $f^{-1.5}$ in the region where it is thermally thin (i.e., between 360 and 580 Hz), an essentially exponential behavior, namely $S \simeq \exp(-a\sqrt{f})/f$, between 640 and 760 Hz, an $f^{-1.0}$ dependence between 800 and 920 Hz, and, finally, an $f^{-1.5}$ behavior between 1.0 and 1.4 kHz. In contrast, the modulation frequency dependence of the signal amplitude for the solar cell with BSF, shown, in Fig. 9, exhibits no intermediate $f^{-1.0}$ dependence as in Fig. 8. In other words, the amplitude varies as $f^{-1.5}$ in the thermally thin region (up to roughly 700 Hz), varies as $\exp(-a\sqrt{f})/f$ in the beginning of the thermally thick region, between 800 and 1000 Hz, and finally varies as $f^{-1.5}$ again deep into the thermally thick region above 1 kHz.

Finally, in Figs. 10 and 11 we show the OPC signal amplitude of sample 5 and 6, respectively, as a function of the modulation frequency in the region where both samples are thermally thick. Actually, in Figs. 10 and 11 we have plotted the dependence of the product of the signal amplitude times $f^{1.5}$ on the modulation frequency, since in this frequency range both samples exhibited a slight deviation from the $f^{-1.5}$ modulation frequency dependence at the same time that their signal phase angles remained monotonically decreasing with increasing modulation frequency.

DISCUSSIONS AND CONCLUSIONS

To explain the behavior of our semiconducting samples we resort to the thermal-piston model of Rosencwaig and Gersho (RG), from which the pressure fluctuation δP in the PA cell, due to the periodic heating of the sample, is given by[13]

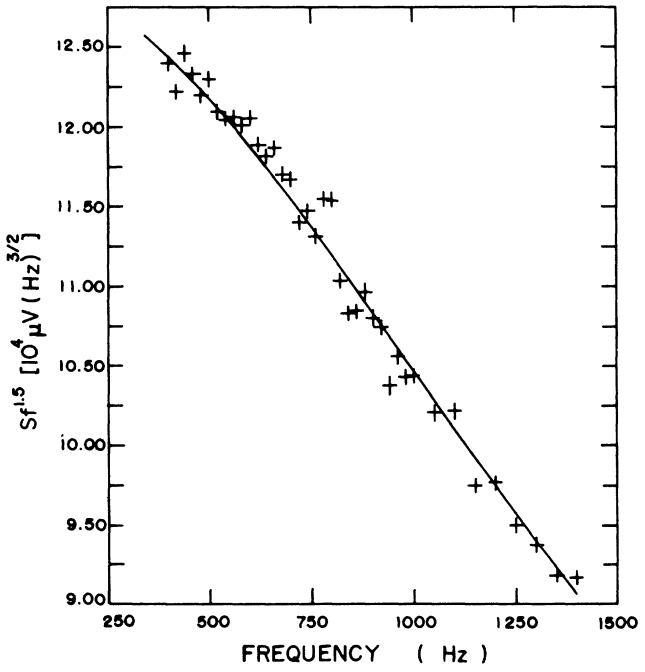

FIG. 10. The OPC signal amplitude of the sample 5 times $F^{1.5}$ as a function of the modulation frequency. The solid line represents the data fitting to Eq. (13) of the text.

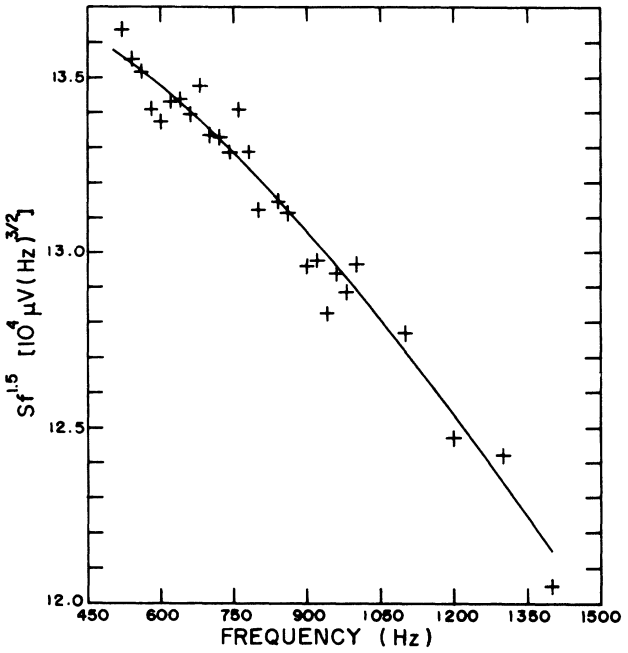

FIG. 11. The OPC signal amplitude of the sample 6 times $f^{1.5}$ as a function of the modulation frequency. The solid line represents the data fitting to Eq. (13) of the text.

$$\delta P = \frac{P_0 \theta}{T_0 l_g \sigma_g} e^{j\omega t} , \tag{1}$$

where P_0 (T_0) is the ambient pressure (temperature), l_g is the length of the gas chamber, $\sigma_g = (1+j)a_g$, $a_g = (\pi f/\alpha_g)^{1/2}$ is the thermal diffusion coefficient in the gas with thermal diffusivity α_g, and θ is the sample temperature fluctuation at the $x = 0$ sample-gas interface. In the remaining we are considering the PA cell geometry for the heat-transmission configuration shown schematically in Fig. 1(b). The temperature fluctuation θ is obtained from the solution to the thermal diffusion equation, namely,

$$\frac{\partial^2 T}{\partial x^2} = \frac{1}{\alpha_s}\frac{\partial T}{\partial t} - \frac{Q(x,t)}{k_s} , \tag{2}$$

where α_s (k_s) is the sample thermal diffusivity (conductivity), and $Q(x,t)$ is the heat power density generated in the sample due to the absorption of light. The thermal power density $Q(x,t)$ may be regarded as due to three different processes.[3] (i) An instantaneous intraband nonradiative thermalization with energy greater than E_g. This process, due to the electron-phonon collisions within the conduction band, occurs in a time scale of picoseconds and may be assumed instantaneous in the typical range of modulation frequencies of photoacoustics. The heat power density due to this process, denoted by Q_D, is then[13]

$$Q_D = \frac{\beta(h\nu - E_g)}{h\nu} I_0 e^{\beta(x+l_s)} e^{j\omega t} , \tag{3}$$

where β is the optical-absorption coefficient for photons of energy $h\nu$, incident $x=-l_s$ at the $x=-l_s$ surface with an intensity of $I_0(\mathrm{W/cm^2})$. (ii) Nonradiative bulk recombination. This process is due to the excess electron-hole pairs recombination after diffusing a distance $(D\tau)^{1/2}$, where D is the carrier diffusion coefficient, and τ is the band-to-band recombination time. The heat power density, Q_{NRR}, for this process is

$$Q_{\mathrm{NRR}}=\frac{E_g}{\tau}n(x,t)\ , \tag{4}$$

where $n(x,t)$ is the density of photoexcited excess carriers. (iii) Nonradiative surface recombination. The heat power density, Q_{SR}, due to the nonradiative carrier recombination at the sample surface is written as

$$Q_{\mathrm{SR}}=E_g[v\delta(x)+v_0\delta(x+l_s)]n(x,t)\ , \tag{5}$$

where v_0 is the carrier surface recombination velocity at the back (heating) surface, and v is the surface recombination velocity at the sample-gas interface at $x=0$.

The above discussion means that the solution to Eq. (2) depends explicitly on $n(x,t)$, which, in turn, obeys the carrier diffusion equation, namely,

$$\frac{\delta n}{\partial t}=D\frac{\partial^2 n}{\partial x^2}-\frac{n}{\tau}+\frac{\beta I_0}{h\nu}e^{(x+l_s)}e^{j\omega t}-vn(x,t)\delta(x) -v_0 n(-l_s,t)\delta(x+l_s)\ . \tag{6}$$

For the case of short-wavelength incident radiation, as in the case of our experiments, we may assume that all the incident radiation is being absorbed at the $x=-l_s$ surface; this corresponds to formally replacing the term $\beta I_0 e^{\beta(x+l_s)}$ by $I_0(x+l_s)$ in Eqs. (3) and (6). Making this assumption and neglecting the heat flux into the surrounding gas, the solution to the coupled equations (2) and (6) leads to the following expression for the pressure fluctuation for thermally thick sample:[14]

$$\delta P=\frac{2\epsilon I_0 P_0}{T_0 l_g\sigma_g k_s\sigma_s}\left[\left(\frac{\epsilon-1}{\epsilon}\right)e^{-l_s\sigma_s} +\frac{F\sigma_s}{D\gamma\tau}\left(\frac{1}{\sigma_s^2-\gamma^2}+\frac{v\tau}{\sigma_s}\right)\right]\ , \tag{7}$$

where $\sigma_s=(1+j)a_s$, $a_s=(\pi f/\alpha_s)^{1/2}$ is the thermal diffusion coefficient of the sample, $\gamma=(1/D\tau)^{1/2}(1+j\omega\tau)^{1/2}$ is the carrier diffusion coefficient, $\epsilon=E_g/h\nu$, $r=v/D\gamma$, $r_0=v_0/D\gamma$, and

$$F=\frac{1}{(1+r_0)(1+r)e^{\gamma l}-(1-r)(1-r_0)e^{-\gamma l}}\ . \tag{8}$$

The neglect of the heat flux into the surrounding gas, as implied in Eq. (7), is justified by the fact that the air thermal conductivity is much smaller than that of most materials. This is a widely used approximation in the photothermal theories and corresponds to neglecting the factor $g=(k_g/k_s)(\alpha_s/\alpha_g)^{1/2}$ of RG model[13] as compared to unity. The condition of thermally thick sample, which corresponds to the experimental situation discussed in this paper, means that $l_s\sigma\gg 1$. The first term in Eq. (7), scaling exponentially with the modulation frequency as $(1/f)\exp(-a\sqrt{f}\,)$, where $a=l_s(\pi/\alpha_s)^{1/2}$, is the usual thermal diffusion contribution from an instantaneous heat source, as described by the RG model. As to the contributions from the nonradiative recombination terms in Eq. (7) one has to distinguish between two cases. One is when the nonradiative band-to-band recombination time is small enough such that in the frequency range of the experiment $\omega\tau\ll 1$. In this case we may approximate γ as $\gamma\simeq(D\tau)^{-1/2}$ so that the parameters r, r_0, and F all become real constants independent of the modulation frequency. In this case the second term in the square brackets of Eq. (7), in the high-frequency regime such that $\sigma_s^2>\gamma^2$, scales as $f^{-1.5}$ (it is the contribution from the nonradiative bulk recombination), whereas the last term in Eq. (7) varies as $f^{-1.0}$ (it is the contribution from the nonradiative surface recombination). Thus, the overall modulation frequency dependence of the PA signal for a thermally thick semiconductor in the heat-transmission configuration, in the frequency range such that $\omega\tau\ll 1$, is such that it initially varies exponentially as $\exp(-a\sqrt{f}\,)$, as in the usual case of an instantaneous heat source. As we move deep into the thermally thick regime, the instantaneous heat source weakens exponentially and the PA signal becomes dominant by the nonradiative (slow) bulk and surface recombination processes. In this regime, the PA signal varies as $f^{-1.5}$, due to the bulk nonradiative recombination processes, and at higher modulation frequency it scales as $f^{-1.0}$, due to the surface recombination contribution. The above conclusions seem to explain the behavior of the OPC signal amplitude of our GaAs samples, shown in Figs. 2–5. In fact, for samples 1–3, having fast carrier recombination velocities at the rear surface (i.e., v large), the signal amplitude varies as $f^{-1.5}$ and changes its modulation frequency dependence to $f^{-1.0}$ at high frequencies. At the same time, their phase angles, as seen in Figs. 6 and 7, exhibit minima at the modulation frequencies where the signal amplitude changes from the $f^{-1.5}$ to the $f^{-1.0}$ frequency dependence. We note that due to a larger signal-to-noise ratio the data fitting shown in Fig. 6 (sample 1) looks better than that of Fig. 7 (sample 2). In contrast, sample 4, having a small carrier recombination velocity v, always exhibits an $f^{-1.5}$ frequency dependence as shown in Fig. 5. We therefore conclude that the OPC signal for the GaAs samples in the thermally thick region is essentially determined by the nonradiative recombination processes. In fact, considering only the second and third terms of Eq. (7), namely,

$$\delta P=\frac{2\epsilon f_0 P_0 F}{T_0 l_g k_s D_\gamma\tau\sigma_g}\left(\frac{1}{\sigma_s^2-\gamma^2}+\frac{v\tau}{\sigma_s}\right)\ , \tag{9}$$

and still assuming that $\omega\tau\ll 1$, we can show that the phase angle of the OPC signal is given by

$$\phi=\frac{\pi}{2}+\Delta\phi\ , \tag{10}$$

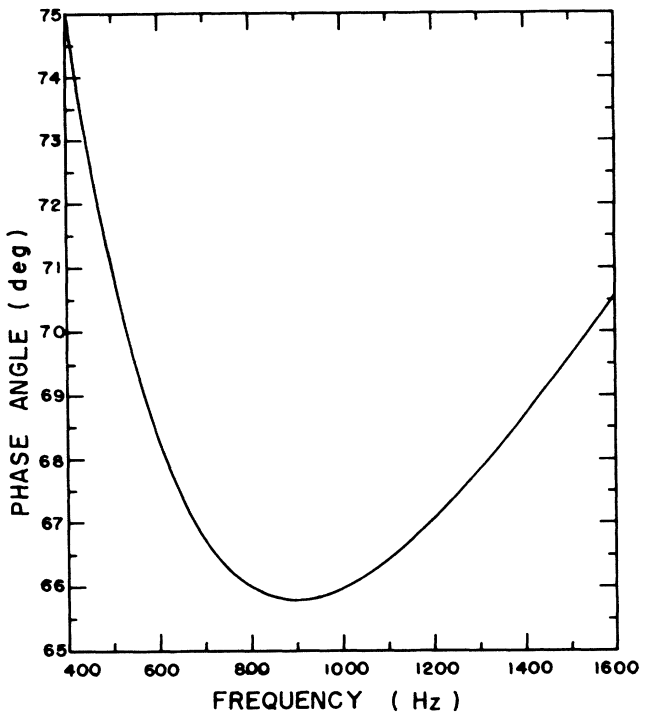

FIG. 12. Variation of the phase angle $\Delta\phi$, given by Eq. (11) of the text, as a function of the modulation frequency, for a typical n-type GaAs sample with $\tau_{\text{eff}}=5.7$ μs and $v=490$ cm/s.

where

$$\tan\Delta\phi=\frac{(aD/v)(\omega\tau_{\text{eff}}+1)}{(aD/v)(1-\omega\tau_{\text{eff}})-1-(\omega\tau_{\text{eff}})^2}\ , \tag{11}$$

with $\tau_{\text{eff}}=\tau[(D/\alpha_s)-1]$ and $a=(\pi f/\alpha_s)^{1/2}$. In Fig. 12 we plot the variable part of the phase angle $\Delta\phi$ as a function of the modulation frequency using the values of D and α corresponding to a typical n-type GaAs sample, namely, 6 and 0.40 cm^2/s, respectively, and for $\tau=5.7\mu_s$ and $v=490$ cm^2/s. Figure 12 shows that on increasing the modulation frequency the phase angle initially decreases, reaches a minimum, and then increases on further increasing the modulation frequency. The breaking frequency at which $\Delta\phi$ exhibits a minimum corresponds roughly to the point at which the signal changes from the $f^{1.5}$ to the $f^{-1.0}$ behavior. That is, it marks the transition from the bulk to the surface recombination process, as being the dominant mechanism responsible for the PA signal.

Using Eqs. (10) and (11) for the OPC phase angle we have carried out the data fitting for sample 1–3 in the frequency range of our measurements, leaving as adjustable parameters D, v, α, and τ. The results of the best fit to the data are represented in Figs. 6 and 7 by the solid lines for samples 1 and 2, respectively. In Table II we summarize the values found for the adjusted parameters for samples 1–3. The values of the carrier diffusion coefficient shown in Table II for samples 2 and 3 are quite close to the room-temperature value of the minority carrier (hole) diffusion coefficient for an n-type GaAs sample with a doping concentration of about 10^{18} cm^{-3}. In fact, using the literature value[15] for the hole mobility for a doping concentration of 10^{18} cm^{-3}, namely, $\mu_h\simeq 170$ cm^2/s, one gets for $D_h=k_\beta T\mu_h/e$ a value of 4.4 cm^2/s, which is in good agreement with those values found from the data fitting for samples 2 and 3. In contrast, for sample 1 the value of D in Table II is quite close to the ambipolar diffusion coefficient, namely, $D_a=2k_\beta\tau\mu_e\mu_h/e(\mu_e+\mu_h)$, for the doping concentration of 5.2×10^{17} cm^{-3}. At this doping level one has for the carrier mobilities[15] $\mu_e\simeq 3500$ cm^2/s and $\mu_h\simeq 200$ cm^2/s. This leads to $D_a=9.8$ cm^2/s, which agrees quite well with the value shown in Table II for sample 1. This result is not surprising since in the case of sample 1 we have used a 180-mw Ar^+-ion laser as the heating beam which generates large photoinjected carrier population. It is well known[15–17] that for large photoinjected carrier population (i.e., $\Delta n \gg N_I$, where N_I is the impurity concentration) the carrier diffusion is dominated by the ambipolar diffusion, whereas for the small photoinjected carrier population the carrier diffusion is dominated by the minority carriers. As for the values obtained for the thermal diffusivity, as shown in Table II, they agree very well with the literature value[12] of 0.40 cm^2/s for GaAs. Finally, we note that for sample 1 the value found for the surface recombination velocity was greater than the corresponding ones for samples 2 and 3. This is physically expected since the rear surface for sample 1 had an annealed Au film which is known[12,15] to increase considerably the density of the surface recombination centers.

The dependence of the solar cell data on the modulation frequency seems also to be well described by the above model. In fact, the main difference between the solar-cell data with and without BSF shown in Figs. 9 and 8, respectively, is the absence of the $f^{-1.0}$ modula-

TABLE II. Values of the physical parameters for the GaAs samples obtained from the phase angle data fitting as given by Eqs. (10) and (11) of the text.

	Sample	Diffusion coefficient (cm^2/s)	Thermal diffusivity (cm^2/s)	Surface recombination velocity (cm/s)	Relaxation time (μs)
n-type GaAs	1	9.10	0.38	580.7	6.05
n-type GaAs	2	5.71	0.39	489.1	5.72
n-type GaAs	3	4.23	0.42	436.3	5.48

tion frequency dependence in the case of the solar cell with BSF (cf. Fig. 9). As discussed above the $f^{-1.0}$ contribution is essentially due to the surface recombination process and therefore it should be of no effect when the solar cell has a BSF. The $f^{-1.5}$ frequency dependence in the low-modulation frequency region is, of course, the usual one[10,11,14] for a thermally thin sample in the heat-transmission configuration of the OPC measurements. Finally the exponentially decaying signal in the beginning of the thermally thick region in Figs. 8 and 9 is due to the instantaneous intraband heat source as given by the first term of Eq. (7). The fit of the experiment in this modulation frequency range to an expression of the form $(1/f)\exp(-a\sqrt{f})$, where $a=l_s(\pi/\alpha_s)^{1/2}$, allows us to find the parameter a. Knowing a we can then calculate the thermal diffusivity α_s. The results we got for α_s from this data fitting were $\alpha_s=0.96$ cm^2/s for the cell without BSF, and $\alpha_s=1.03$ cm^2/s for the solar cell with BSF. These values for the thermal diffusivity are in good agreement with the literature values[12,15] of the thermal diffusivity of Si, namely $\alpha_s=0.85-1.06$ cm^2/s.

In contrast to the previous cases, the p-type Si samples (5 and 6) exhibited an $f^{-1.5}$ modulation frequency dependence up to roughly 700 Hz; at higher frequencies the power-law frequency dependence begins to deviate from the 1.5 exponent towards higher values of the exponent. This is shown in Figs. 10 and 11 for samples 5 and 6, respectively. At the same time, the OPC signal phase angle of both samples exhibited only a slight decrease in the entire frequency range. To understand this behavior we have assumed that the bulk nonradiative band-to-band recombination process is the dominant mechanism responsible for the observed signal. This is consistent with the observed $f^{-1.5}$ frequency dependence in the thermally thick region together with the fact that no tendency to follow an $f^{-1.0}$ power law at high frequencies was evident. We next relaxed the previous assumption that $\omega\tau$ is much smaller than 1, and assumed that $\omega\tau\gg1$ so that the parameter r may be written as $r\simeq(1+j)(\pi f/D)^{1/2}$. This is a more appropriate assumption for an indirect-gap semiconductor at high modulation frequencies.

Under these assumptions, the pressure fluctuation in the OPC configuration is given by the first term in Eq. (9), namely,

$$\delta P_{\mathrm{NRR}}=\frac{2\epsilon I_0 P_0}{T_0 l_g \sigma_g k_s \tau D\gamma\sigma_s^2}\,\frac{1}{(1+r)(1+r_0)e^{\gamma l}-(1-r)(1-r_0)e^{-\gamma l}}\ , \tag{12}$$

where we have substituted $\sigma_s^2-\gamma^2$ by σ_s^2 since, for Si, the thermal diffusivity α_s is much smaller than the carrier diffusion coefficient D. Using the typical values of D for Si one can show that for the thicknesses of samples 5 and 6, γl is smaller than 1 even at the highest modulation frequencies used in our experiments. Thus, expanding in Eq. (12) $\exp(\pm\gamma l)$ as $1\pm\gamma l$ and performing some tedious but straightforward calculations, the band-to-band nonradiative recombination signal amplitude reduces to

$$|\delta P|=\frac{\epsilon P_0 I_0 D\alpha_g^{1/2}\alpha_s}{(2\pi)^{3/2}T_0 l_g k_s\tau}\,\frac{1}{f^{1.5}[a^2+(bf)^2]^{1/2}}\ , \tag{13}$$

where

$$a=D(v+v_0)+lvv_0\ , \tag{14a}$$

and

$$b=2\pi lD\ . \tag{14b}$$

Equation (13) implies that on increasing the modulation frequency, the OPC signal amplitude should deviate from the $f^{-1.5}$ power law towards a faster decreasing behavior. Using Eq. (13) we have carried out the signal amplitude data fitting for samples 5 and 6 in the frequency range of our experiments leaving a and b as adjustable parameters. The results of the best fit to the data are shown in Figs. 10 and 11 by the solid lines. For example, for the PS-RS sample (5) the value of b obtained from the best fit was 4.47, which for a thickness of 388 μm gives us $D=18.3$ cm^2/s. To estimate the rear surface recombination velocity v we note that for a PS-RS sample, $v_0\ll v$, so that the expression for the fitting parameter a [cf., Eq. (14a)] may be approximated by $a\simeq Dv$. Thus, using the value of D obtained from b we can find v from $a=Dv$. For sample 5, v was found to be 334.6 cm/s. Now, for the RS-RS sample (6), having both surfaces equally prepared, we may set $v_0=v$ so that Eq. (14a) reduces to

$$a=lv^2+2Dv \quad\text{or}\quad v=-\frac{D}{l}+\frac{1}{l}(D^2+la)^{1/2}\ . \tag{15}$$

This means that having got D from the value of b from the best fit we can find v from Eq. (15) for the RS-RS for sample. In Table III, we summarize the values found for D and v from the signal amplitude data fitting for samples 5 and 6. We first note from Table III that, for both sam-

TABLE III. Values of the diffusion coefficient and the rear surface recombination velocity for the p-Si samples obtained from the bulk nonradiative recombination signal amplitude as given by Eq. (13) of the text.

Sample	Surface state	Diffusion coefficient (cm^2/s)	Surface recombination velocity (cm/s)
5	PS-RS	18.3	334.6
6	RS-RS	34.1	331.5

ples, the values of v for the roughened surfaces are in close agreement with each other. This is expected since both rear surfaces were equally prepared. As for the values of D, however, the results we got were such that for the PS-RS sample D corresponds to the ambipolar diffusion coefficient, whereas for the RS-RS sample D is quite close to the minority (electron) diffusion coefficient. This result is the same as the one obtained for the n-type GaAs samples previously discussed; for PS-RS samples we have high photoinjected carrier density so that the carrier diffusion is essentially dominated by the ambipolar diffusion while for the light beam incident upon a roughened surface, as in the case of RS-RS samples, the carrier diffusion is dominated by the minority carriers due to the small carrier density photoinjected into the bulk. In fact, for Si the electron and hole mobilities may be expressed in terms of the doping concentration $N(\mathrm{cm}^{-3})$ by the following empirical formula:[18]

$$\mu_e = 65 + \frac{1265}{1 + \left[\frac{N}{8.5}10^{-16}\right]^{0.72}} \ \mathrm{cm}^2/\mathrm{V\,s}\ , \tag{16a}$$

$$\mu_h = 47.7 + \frac{447.3}{1 + \left[\frac{N}{6.3}10^{-16}\right]^{0.76}} \ \mathrm{cm}^2/\mathrm{V\,s}\ . \tag{16b}$$

For the doping concentration for the p-type Si samples shown in Table I one gets from Eqs. (16), $\mu_e = 1316.96$ $\mathrm{cm}^2/\mathrm{V\,s}$ and $\mu_h = 409.51$ $\mathrm{cm}^2/\mathrm{V\,s}$, from which we get $D_a = 18.5$ cm^2/s and $D_e = 34.1$ cm^2/s. These values for diffusion coefficients are in very good agreement with those obtained from the data fitting shown in Table III.

In conclusion, we believe we have demonstrated the usefulness of the OPC detection, which corresponds to an enhanced signal-to-noise ratio heat transmission PA detection, for characterizing the thermal and carrier transport properties of semiconductors. It was shown that the modulation frequency scanning of the OPC signal amplitude and phase in the frequency range where the sample is thermally thick can single out the different fast and slow nonradiative recombination heat sources responsible for the PA signal. At the same time the experiments reported in this work suggest a practical procedure for the measurement of the surface recombination velocity and of the carrier diffusion coefficient (and, therefore, the mobility). This procedure is essentially based upon the recording of the OPC signal as a function of the modulation frequency, in the thermally thick region, for two different combination of surface treatments, namely, a PS-RS and a RS-RS surface treatments. In the PS-RS case the carrier diffusion is essentially dictated by the ambipolar diffusion due to a large carrier density photoinjected into the sample, whereas for the RS-RS surface treatment the carrier diffusion is dominated by the minority carrier diffusion. Knowing the ambipolar and the minority carrier diffusion, the majority carrier diffusion coefficient (and, therefore, the mobility) is straightforwardly obtained. Furthermore, if the nonradiative recombination time τ is sufficiently small, such that $\omega\tau \ll 1$, the OPC signal phase should exhibit a minimum as a function of the modulation frequency. The data fitting in this case provides us the values of both v and τ. This is usually the case of direct-band-gap semiconductors. In contrast with sufficiently long relaxation times, the surface recombination velocity is obtained from the deviation of the OPC signal amplitude from the $f^{-1.5}$ frequency dependence as in the case of the Si samples discussed above.

[1] W. L. Smith, A. Rosenewaig, D. L. Willenborg, J. Opsal, and M. W. Taylor, Solid State Technol. **29**, 85 (1986).

[2] A. Mandelis, *Photoacoustic and Thermal Wave Phenomena in Semiconductors* (North-Holland, New York, 1987).

[3] H. Vargas and L. C. M. Miranda, Phys. Rep. **161**, 43 (1988).

[4] L. Eaves, H. Vargas, and P. J. Williams, Appl. Phys. Lett. **38**, 768 (1981).

[5] I. N. Bandeira, H. Closs, and C. C. Ghizoni, J. Photoacoust. **1**, 275 (1982).

[6] L. C. M. Miranda, Appl. Opt. **21**, 2923 (1982).

[7] N. Mikoshiba, H. Nakamura, and K. Tsubouchi, in *Proceedings of the IEEE Ultrasonics Symposium, San Diego, 1982* (IEEE, New York, 1982), p. 580.

[8] V. A. Sablikov and V. B. Sandomirskii, Phys. Status Solidi **120**, 471 (1983); Fiz. Tekh. Poluprovodn. **17**, 81 (1983) [Sov. Phys.—Semicond. **17**, 50 (1983)].

[9] A. N. Vasilev and V. B. Sandomirskii, Fiz. Tekh. Poluprovodn. **18**, 1951 (1984) [Sov. Phys.—Semicond. **18**, 1095 (1984)]; **18**, 1954 (1984) [**18**, 1221 (1984)].

[10] M. D. Silva, I. N. Bandeira, and L. C. M. Miranda, J. Phys. E **20**, 1476 (1987).

[11] L. F. Perondi and L. C. M. Miranda, J. Appl. Phys. **62**, 2955 (1987).

[12] A. S. Grove, in *Physics and Technology of Semiconductor Devices* (Wiley, New York, 1964), p. 102.

[13] A. Rosencwaig and A. Gersho, J. Appl. Phys. **47**, 64 (1976).

[14] A. Pinto Neto, H. Vargas, N. F. Leito, and L. C. M. Miranda, Phys. Rev. B **40**, 3924 (1989).

[15] S. M. Sze, in *Physics of Semiconductor Devices* (Wiley, New York, 1969), p. 57.

[16] R. G. Stearms and G. S. Kino, in *Photoacoustic and Thermal Wave Phenomena in Semiconductors* (North-Holland, Amsterdam, 1987), p. 201.

[17] J. S. Blakemore, *Semiconductor Statistics* (Pergamon, New York, 1962).

[18] M. A. Green, *Solar Cells* (Prentice Hall, New Jersey, 1982).